Published in Marine Geology 201 : 147-168, 2003,
which should be used for any reference to this work

Investigating the history of East Asian monsoon and climate during the last glacial–interglacial period (0–140 000 years): mineralogy and geochemistry of ODP Sites 1143 and 1144, South China Sea

F. Tamburini [a,*], T. Adatte [a], K. Föllmi [a], S.M. Bernasconi [b], P. Steinmann [a]

[a] *Institut de Géologie, Université de Neuchâtel, 2007 Neuchâtel, Switzerland*
[b] *Geological Institute, ETH-Zentrum, 8092 Zürich, Switzerland*

Abstract

Monsoon climate is an important component of the global climatic system. A comprehensive understanding of its variability over glacial–interglacial time scales as well as of its effects on the continent and in the ocean is required to decipher links between climate, continental weathering and productivity. A detailed multiproxy study, including bulk and clay mineralogy, grain-size analysis, phosphorus geochemistry (SEDEX extraction), organic matter characterization, and nitrogen stable isotopes, was carried out on samples from ODP Sites 1143 and 1144 (Leg 184, South China Sea), covering the past 140 000 years. We tentatively reconstruct the complex sedimentation and climatic history of the region during the last glacial–interglacial cycle, when sea-level variations, linked to the growth and melting of ice caps, interact with monsoon variability. During interglacial periods of high sea level, summer monsoon was strong, and humid and warm climate characterized the adjacent continent and islands. Clay minerals bear signals of chemical weathering during these intervals. High calcite and reactive phosphorus mass accumulation rates (MARs) indicate high productivity, especially in the southern region of the basin. During glacial intervals, strong winter monsoon provided enhanced detrital input from the continent, as indicated by high detrital MAR. Glacial low sea level resulted in erosion of sediments from the exposed Sunda shelf to the south, and clay mineral variations indicate that warm and humid conditions still prevailed in the southern tropical areas. Enhanced supply of nutrients from the continent, both by river and eolian input, maintained high primary productivity. Reduced circulation during these periods possibly induced active remobilization of nutrients, such as phosphorus, from the sediments. Intense and short cold periods recorded during glacial and interglacial stages correlate with loess records in China and marine climatic records in the North Atlantic, confirming a teleconnection between low- and high-latitude climate variability.

Keywords: South China Sea; Pleistocene–Holocene climate; monsoon; continent–ocean interaction; phosphorus geochemistry

* Corresponding author. Present address: Geological Institute, ETH-Zentrum, Zürich CH-8092, Switzerland.
E-mail addresses: thierry.adatte@unine.ch (T. Adatte), karl.foellmi@unine.ch (K. Föllmi), stefano@erdw.ethz.ch (S.M. Bernasconi), philipp.steinmann@unine.ch (P. Steinmann).

1. Introduction

The South China Sea (SCS), with a total area of 3.5×10^6 km^2, represents one of the largest marginal basins in the Pacific. The SCS is sensitive to changes in East Asian monsoon intensity and duration, to changes in detrital input (river/eolian) from the continent, as well as to variations in atmospheric and oceanic circulation and exchanges with the open Pacific ocean (Wang et al., 2000). Moreover, the SCS is highly suitable to study and reconstruct relationships between continental weathering, productivity and climate, as the basin receives detrital fluxes from three of the largest rivers in the world (Mekong river in the south, Red and Pearl rivers in the North; Fig. 1).

The primary objective of ODP Leg 184 was to obtain records of the climatic and paleoceanographic history of the SCS (Wang et al., 2000). The goals of this multiproxy study are: (i) to decipher changes in the sedimentation history of the SCS related to variations in monsoon regime, (ii) to understand patterns and gradients in detrital material distribution and nutrient concentration between the northern and the southern SCS, and (iii) to obtain a better insight into connections between monsoon and climate variations, continental weathering and productivity, during the last glacial–interglacial cycle (140 000 years). Bulk and clay mineralogy, organic matter analyses, grain-size analysis, nitrogen stable isotope analyses, and determination of four sedimentary phosphorus reservoirs have been performed. The investigated samples are from ODP Sites 1143 and 1144, drilled in the southern and northern regions of the SCS, respectively (Fig. 1).

1.1. East Asian monsoon

The Asian monsoon is a major component of the climate system. An important teleconnection between the Asian monsoon and high-latitude climate is suggested by the correlation between low- (e.g. SCS and Arabian Sea) and high-latitude records (e.g. GRIP; Sirocko et al., 1996; Wang and Oba, 1998; An, 2000). Monsoon circulation results from the heating capacity contrast between continent and ocean. This situation, linked to the annual cycle in incoming solar energy, produces extreme seasonality in wind direction, rainfall and temperature patterns over the Asian continent (Webster, 1987). During summer, the formation of a low-pressure cell on the Tibetan plateau contrasts with a high-pressure cell on the Indian Ocean, causing southwesterly winds to blow from the sea to the continent. These winds bring along moisture and heavy rains and promote a humid and hot climate on land. During winter, the low-pressure cell is located on the Indian Ocean and winds blow from the interior of the continent, which is characterized by cold and dry conditions, to the ocean (Fig. 2). The East Asian monsoon is characterized by strong summer and winter monsoonal circulation, unlike the Indian Monsoon, which shows strong summer and weak winter monsoonal circulation (Prell and Kutzbach, 1992; Huang et al., 1997).

1.2. Area description and site location

The SCS is a semi-enclosed marginal sea connected to the East China Sea (ECS) through the Taiwan strait, to the Pacific Ocean through the Bashi strait, to the Sulu Sea through the Mindoro, to the Java Sea through the Gasper and Karimata straits, and to the Indian Ocean through the Malacca strait (Fig. 1). Sea surface circulation is controlled by monsoon activity: during summer, subtropical waters are advected into the SCS through the southern straits. They flow northward along the Indochina and China coasts, following an anticyclonic pattern, and exit the SCS through the Taiwan strait (Wang et al., 1995). This pattern is reversed during winter time, with cold and saline waters entering the SCS from the north. According to (Wang and Wang, 1990) glacial periods are characterized by a marked seasonality of temperature, as much as 9–10°C, while the gradient decreases to 4–6°C during interglacials and interstadials. Summer monsoon sustains upwelling cells along the SE coast of Indochina and the NW coast of the Philippines; their activity might cease or diminish during glacial periods, in relation to weakened SW monsoons.

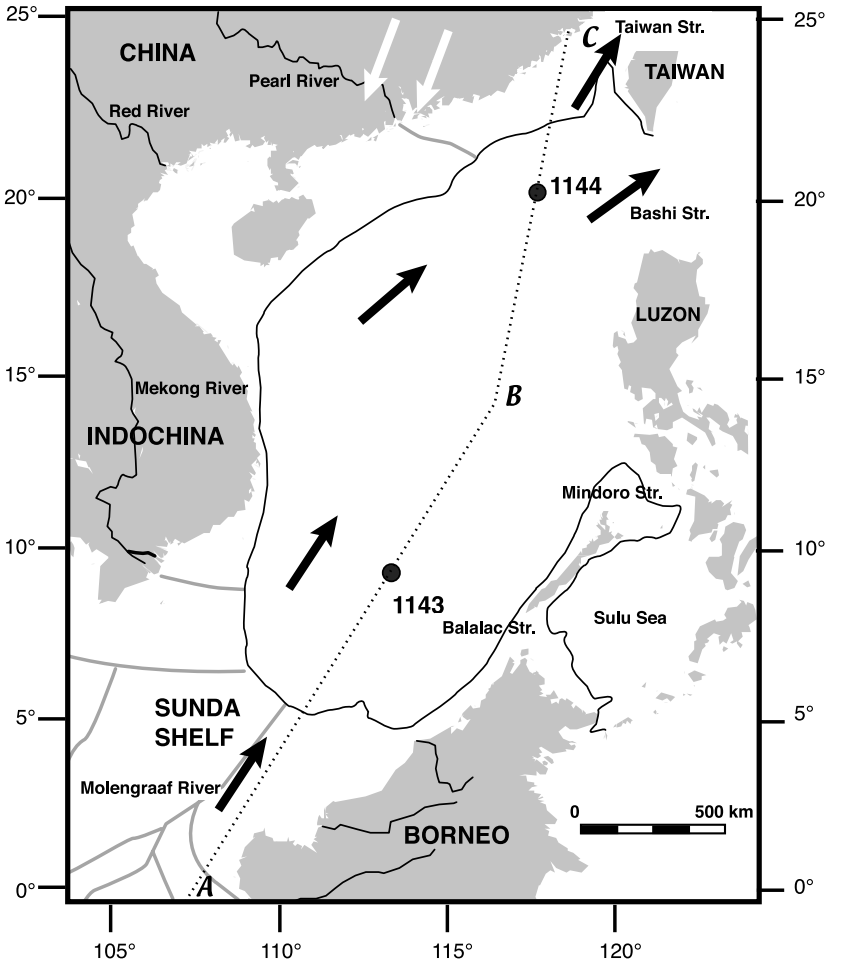

Fig. 1. Map of the SCS and location of ODP Sites 1143 and 1144. Black arrows indicate summer monsoon direction, while white arrows indicate winter monsoon direction. The thick solid line represents the 200 m isobath, considered as the limit between the continental shelf and the slope. The dotted line (ABC) represents the track of the bathimetric profile used in the schematic models of Figs. 10 and 11.

During glacials, the Asian continent experienced cold and dry conditions, as testified by loess accumulation and pollen data (An, 2000), while the southern islands were characterized by a tropical to subtropical climate (Wang et al., 1999). Lowstands of sea level exposed wide areas of the continental shelf of the SCS (Fig. 1). Because of the shallow depth of most of the sills, only the Bashi strait (2500 m water depth) between Taiwan and Luzon remained open during glacials, allowing only the inflow of temperate waters from the Pacific Ocean (Wang and Wang, 1990). The southern SCS was more sensitive to these glacio-eustatic changes, as the emergence of the Sunda shelf closed the connections with the Indian Ocean and allowed the development of a wide drainage system (Molengraaff and Mekong rivers; Pelejero et al., 1999). High nutrient levels were most likely maintained by enhanced input from the continent and the exposed shelf (Schönfeld and Kudrass, 1993; Wang et al., 1999). Weak circulation, increased fluvial discharge in the south, and enhanced accumulation of organic carbon prompted oxygen depletion of intermediate

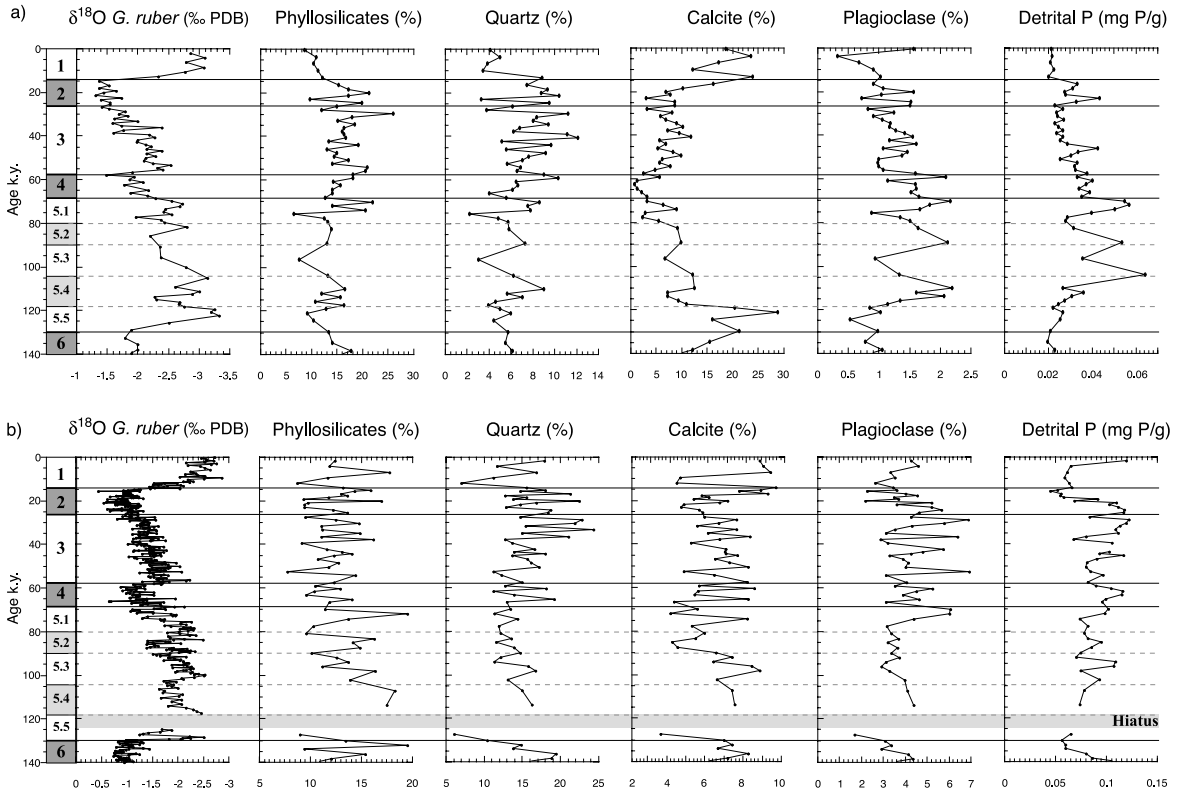

Fig. 2. Percent phyllosilicates, quartz, calcite, K-feldspar and plagioclase and concentration of detrital P of bulk sediment from (a) Site 1143 and (b) Site 1144. Stable oxygen isotope curves for Site 1143 and Site 1144 are taken from Tian et al. (2002) and Bühring et al. (in prep.), respectively. Age is in kyr; MIS are labeled on the left of the graphs. Glacial stages are represented in dark gray, interstadials in light gray and interglacials in white. The gray bar crossing Site 1144 records represents the hiatus recognized using isotopic stratigraphy (see Bühring et al., in prep.).

and bottom waters, especially along the southern coast of the SCS, as deduced by stable carbon isotopes (Wang et al., 1999).

Site 1143 (9°21.72′N, 113°17.11′E, 2777 m water depth) is drilled within a depression of the carbonate platform that forms the southern continental shelf of the SCS, south of the Indochina upwelling region and close to the Mekong river estuary and the Sunda shelf. It is below the Western Pacific Warm Pool, a region of relatively high and stable sea surface temperature (SST). Sediments consist of bioturbated green and gray clay mixed with nannofossil ooze.

Site 1144 (20°3.18′N, 117°25.14′E, 2037 m water depth) is drilled on a sediment drift on the northern continental margin of the SCS, southeast of Hong Kong and of the Pearl River mouth. Bioturbated sediments consist of hemipelagic clay mixed with minor amounts of quartz silt and nannofossil ooze, and are characterized by high organic carbon content and black spots of iron sulfides. This site has an extremely high sedimentation rate (80 cm/kyr for the last 1 Ma; Bühring et al., in prep.).

2. Methods

A total of 132 samples were taken from Sites 1143 and 1144 (61 and 71, respectively), leading to a time resolution averaging 2.5 kyr for Site 1143 and 2 kyr for Site 1144. The stratigraphy of the two sites was inferred by interpolation from the age models of Tian and Wang for Site 1143 (Tian

et al., 2002), and by Buering and Sarnthein for Site 1144 (Bühring et al., in prep.). Based on the isotope stratigraphy, the investigated interval at Site 1143 is continuous, while a hiatus of about 6 kyr has been identified at Site 1144 (Fig. 2; Bühring et al., in prep.).

Analyses were performed at the Geological Institute in Neuchâtel, except for ICP-AES and nitrogen stable isotope analyses, which were performed at the State Environmental Laboratory in Neuchâtel, and at the ETH in Zürich, respectively. All samples were oven-dried at 50°C and divided into subsamples. Five gram of dried sediment was ground to obtain a homogeneous powder <40 μm in size. Clay mineral analyses were based on methods by Kübler (1987). An aliquot of the sample was mixed into de-ionized water (pH 7–8). The carbonate fraction was removed by 10% HCl (1.25 N) at room temperature. The insoluble residue was washed and centrifuged (5–6 times) until a neutral suspension was obtained (pH 7–8). Separation of <2 μm and 2–16 μm size fractions was obtained by the timed settling method based on Stokes' law. XRD analyses of oriented clay samples were made after air-drying at room temperature and ethylene–glycol solvation. Clay mineral relative abundances are given in percent. Smectite contents, measured on the fraction <2 μm treated with glycol, were estimated using the method of Moore and Reynolds (1997). The relative error does not exceed 10%. The geochemical composition and nature of micas and chlorites was determined using ternary diagrams with relative percentages of selected diffraction peaks, as proposed by Rey and Kübler (1983), and Oinuma et al. (1972). The other aliquot was pressed (20 bar) into a powder holder to determine bulk sediment mineralogy by XRD based on a semi-quantitative estimation and using external standards (Kübler, 1987). This method allows quantification of a certain number of mineral species (i.e. quartz, calcite, K-feldspar, plagioclase), while a variable percentage is 'unquantified'. This aliquot is mainly constituted by amorphous minerals (e.g. Fe-oxides and hydroxides), some clay minerals, and organic material. The impossibility of quantitatively determining these mineral components arises from the lack of appropriate standards and from technical complications (for a review, see Kübler, 1987). The relative error of the bulk rock mineralogy is $\sim 5\%$. The relative error on the bulk sediment percentages is about 5%. For both bulk and clay mineralogy analyses a Scintag XRD 2000 diffractometer was used. Grain-size analysis was performed on the insoluble, carbonate-free residues prepared for the clay mineralogy analyses using a Granulometry Laser Oriel CIS. The relative error is 10%. We performed a physical grain-size separation on selected carbonate-free samples, using a Retsch Ultra-Sonic Sieving Apparatus, which allows the separation of five fractions (>60, 35, 20, 10 and 5 μm). The different aliquots of sediments were then visually analyzed with an Environmental Scanning Electron Microscope (ESEM) at the Institute of Microtechnology of the University of Neuchâtel.

The characterization of organic matter was performed on about 100 mg of dried and ground sediment, with a Rock-Eval 6, and using a standard whole-rock pyrolysis method (Espitalié et al., 1986; Lafargue et al., 1996). The method consists of a pyrolysis step (temperature at 300°C for 3 min, then gradual increase to 650°C) and an oxidation step (temperature gradient from 400 to 850°C). Total organic carbon (TOC) is obtained as the sum of four peaks: the S_1 peak (hydrocarbons released at 300°C, FID-curve), the S_2 peak (hydrocarbons produced between 300 and 650°C), the S_3 peak (CO_2 from pyrolysis of organic carbon up to 400°C, IR-curve), and the S_4 peak (CO_2 released from residual organic carbon below ca. 550°C during the oxidation step). The ratio of S_2/TOC (also referred to as hydrogen index HI) is characteristic for the type of organic matter. Nitrogen contents and stable isotopic analyses of the bulk sediment were performed using a Carlo Erba CNS2500 CHN Elemental Analyzer coupled with a Fisons Optima mass spectrometer. Mean errors, calculated as the relative standard deviations on measurements, are about $0.15‰$. All data are reported in the δ notation with respect to atmospheric nitrogen (air ‰). Total nitrogen is here considered as representing the organic nitrogen fraction.

The distribution of sedimentary phosphorus

phases was determined using a four-step sequential extraction technique, adapted from the SEDEX method (Ruttenberg, 1992; Anderson and Delaney, 2000). This method consists of a progressive dissolution of solid phases to extract phosphorus associated with well-defined sedimentary components: iron and manganese oxi-hydroxides, authigenic apatite, detrital apatite and organic matter (Table 1). Phosphorus extracted during the second step of the SEDEX method (see Table 1) mainly accounts for authigenic apatite, fish debris, and for P associated to smectite (Ruttenberg, 1992). In all cases, as dissolved P is removed either from the water column or from the sediments prior to its association to these phases, we could consider and refer to them as authigenic. For all the steps other than the iron-bound P, the ascorbic acid molybdate blue technique was employed to determine P concentrations (Eaton et al., 1995). A Perkin-Elmer UV/Vis spectrophotometer Lambda 10 with a 4-cm quartz cell was used to calculate P concentrations. Concentrations of the iron-bound P phase and ferric Fe were determined using an Optima 3000 Perkin-Elmer ICP-AES. Reagent blanks, standards and consistency standards were used to perform calibration curves for each step and check analytical reproducibility over time.

3. Results

3.1. Bulk sediment mineralogy

Detrital silicate minerals (quartz, phyllosilicates and plagioclase) are present in higher percentages at the northern site (32% on average) than at the southern site (22% on average). K-feldspars, low at both sites (averages 1.06% and 1.33% for Sites 1143 and 1144, respectively), show no significant changes between glacial and interglacial periods, and it is not shown here. Calcite shows high values at Site 1143 (up to 25% of total bulk sediments), while at Site 1144 it is not higher than 10% (Fig. 2).

Site 1143 shows high phyllosilicate contents, up to 45% of total detrital silicates, while quartz represents only 25% of the detrital silicate fraction. Quartz, phyllosilicates, and to a certain extent plagioclase show a quite similar trend, with minima at the beginning of Marine Isotopic Stages (MIS) 5 and 1, and higher values during stages 3 and 2. In contrast to other minerals, calcite at Site 1143 shows important changes between glacial and interglacial values. Maxima are observed at the beginning of stage 5 (30% at 120 ka) and stage 1 (25%), while lowest values are characteristic of stage 4 and, to a lesser extent, of stage 2.

Table 1
Sequential extraction technique applied for phosphorus phase determination (Ruttenberg, 1992; Anderson and Delaney, 2000)

Step name	Treatments	P component isolated	Errors[a]	Detection limits[b]
Iron-bound P	10 ml CBD solution (6 h) (0.22 M sodium citrate, 0.11 M sodium bicarbonate 0.13 M sodium dithionite) 10 ml 1 M $MgCl_2$ (2 h) 10 ml H_2O (2 h)	Exchangeable or loosely sorbed P Reducible or reactive iron-bound P	3–6%	0.03
Authigenic P	10 ml 1 M Na-acetate buffered to pH 4 with acetic acid (5 h) 10 ml 1 M $MgCl_2$ (2 h) 10 ml 1 M $MgCl_2$ (2 h) 10 ml H_2O (2 h)	Carbonate fluorapatite (CFA) biogenic hydroxyapatite	2–7%	0.025
Detrital P	10 ml 1 N HCl (16 h)	Detrital fluorapatite-bound P	3–5%	0.003
Organic P	1 ml 50% (w/v) $MgNO_3$, dry in low oven, ash at 500°C (2 h) 10 ml 1 N HCl (24 h)	Organic-bound P	2–5%	0.004

[a] Typical mean errors for each phase were calculated as the relative standard deviation of the consistency standards.
[b] Detection limits (in mgP/g) for each phase were calculated as three times the standard deviation of blank measurements.

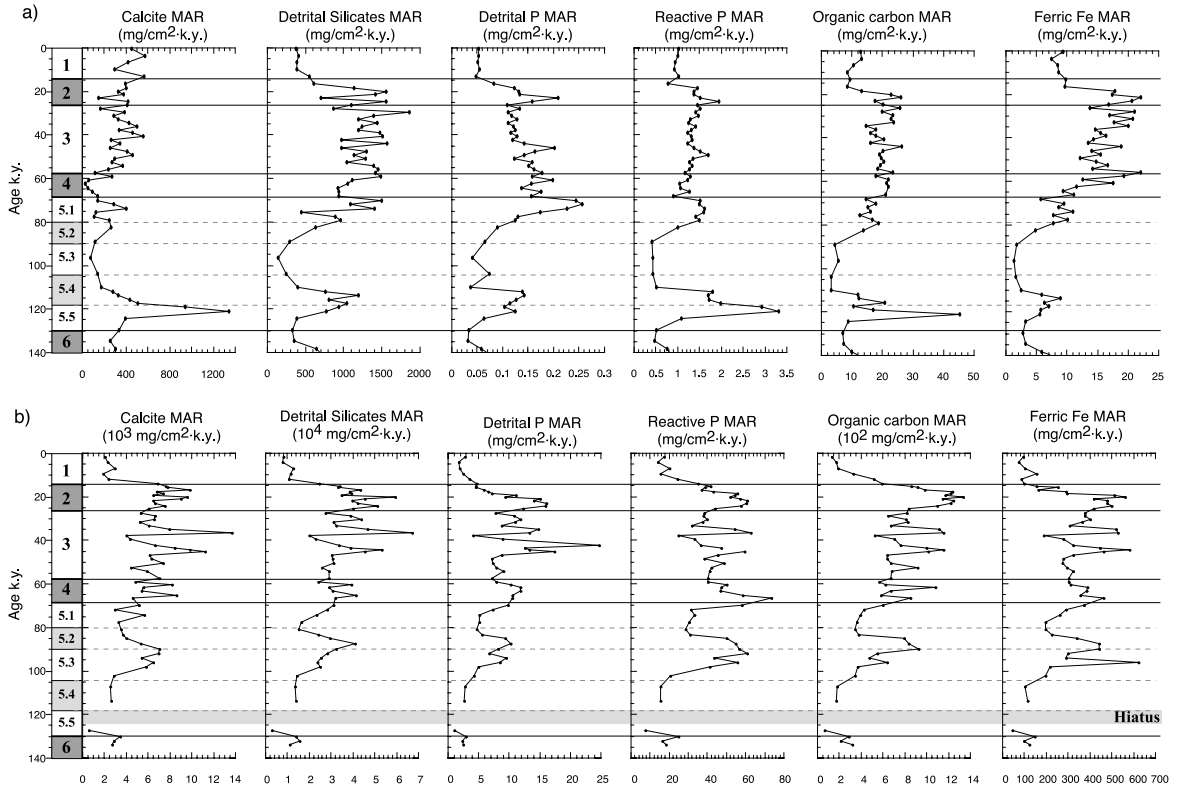

Fig. 3. Mass accumulation rates (MARs) of calcite, detrital silicates, detrital P, reactive P, organic carbon and ferric Fe from (a) Site 1143 and (b) Site 1144. Age and MIS as in Fig. 2. MARs were calculated using the concentration of the different indices as determined by XRD (calcite and detrital silicates), by SEDEX extraction (ferric Fe, detrital and reactive P) and Rock-Eval analysis (organic carbon). Dry bulk density determined onboard and sedimentation rates as inferred from isotopic stratigraphy (Tian et al., 2002; Bühring et al., in prep.) were used. Detrital silicates represent the sum of quartz, phyllosilicates, plagioclase and K-feldspar. Reactive P is the sum of Fe-bound, authigenic and organic-bound P (see text for details).

Quartz is the most abundant mineral at Site 1144, with concentrations reaching about 50% of total detrital silicates (Fig. 2). Two marked minima are present at the beginning of stages 5 and 1, and are paralleled by phyllosilicates, plagioclase, and calcite. Higher values of quartz are found during glacial periods, with peaks of up to 25%. Phyllosilicate percentage remains fairly constant, and averages about 12%. Calcite is generally less than 9% and mirrors the detrital silicate pattern, suggesting a detrital origin.

The presence of iron sulfides and of pyrite was detected at Site 1144 already during onboard description (Wang et al., 2000). The XRD analyses of the bulk sediments and ESEM images reveal the presence of authigenic pyrite at really low percentages (average = 0.11%). Highest values are observed at the top of stage 2.

Mass accumulation rates (MARs) for each proxy are calculated as the product of the concentration of each parameter in mg/g of sediment, the dry bulk density, as recorded onboard during Leg 184, and sedimentation rates, estimated from isotope stratigraphy. Detrital silicate MARs at Site 1143 show a clear glacial–interglacial change, with higher values during MIS 3 and 2, and at the end of stage 5, and minima at the beginning of MIS 5 and 1. MARs of all indices at Site 1144 generally show high variability, due to strong changes in sedimentation rates during the studied interval (Bühring et al., in prep.). MARs are generally higher during MIS 4–2, and at the boundary be-

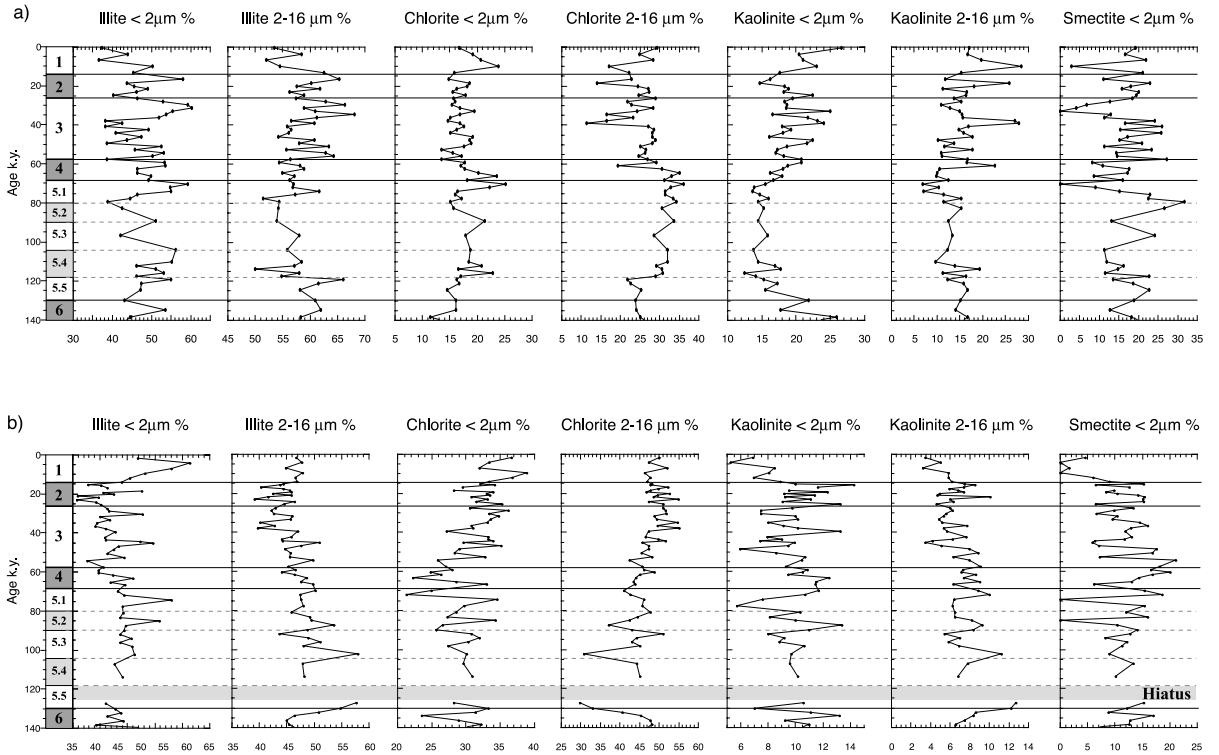

Fig. 4. Relative percentages of illite, chlorite, kaolinite (fractions 2–16 and <2 μm) and smectite (fraction >2 μm) from (a) Site 1143 and (b) Site 1144. Age and MIS as in Fig. 2.

tween stages 5.3 and 5.2. The boundary between stages 2 and 1 is marked by a significant drop in sedimentation rates, which dominates the different MAR records, except for ferric Fe MAR and detrital P (Fig. 3).

3.2. Clay mineralogy (<2 and 2–16 μm fraction mineralogy)

Illite is the most abundant clay mineral at Site 1143, representing on average 45% and 60% of the <2 and 2–16 μm fractions, respectively (Fig. 4). Higher values of illite in the 2–16 μm fraction are observed during MIS 3 and 2, and in the <2 μm fraction at the lower boundaries of glacials. Chlorite is quite abundant, averaging 15% and 25% of the <2 and 2–16 μm fractions, respectively. Kaolinite abundance (2–16 μm fraction) is rather constant throughout the core, with values averaging 15%. The <2 μm kaolinite content shows an increasing trend starting at the beginning of stage 4 and reaching the highest values during MIS 3, at around 40 ka (25%). High values are also recorded in the Holocene section of the core. Smectite presents a scattered pattern: high values, up to 25–30%, are recorded during MIS 5 and the base of stages 3 and 2. A different picture is present at Site 1144, where illite and chlorite represent the most abundant clay minerals of the 2–16 μm and <2 μm fractions, averaging 50% and 45%, respectively (Fig. 4). Kaolinite and illite (2–16 μm fraction) show a decreasing trend from the base of stage 5. Chlorite (<2 μm fraction) shows nearly invariable values during stage 5 and starts increasing at the base of stage 3. A minimum in chlorite (2–16 μm fraction) characterizes stage 5.5. Smectite represents on average 15% of clays of the <2 μm fraction.

The relative percentages of selected diffraction peaks for micas and chlorite were used and plotted in ternary diagrams (not shown) to determine their geochemical composition, as proposed by

Rey and Kübler (1983) for micas and by Oinuma et al. (1972) for chlorites. No differences in the composition of micas and chlorites are observed between glacial and interglacial samples and between the two sites. The <2 μm fraction is mainly constituted by illite–phengite micas, while the coarser-fraction composition is shifted toward the muscovite pole. Chlorites at both sites are enriched in iron concentrated in the silicate layers.

Illite crystallinity in sediments not affected by strong burial can be considered as a proxy, indicating (1) the degree of weathering (hydrolysis) of clay minerals, and/or (2) the nature of the detrital illite (i.e. poorly crystallized illite from soils versus well crystallized illite from lithic sources). This parameter is calculated using the width of the illite peak at 10 Å, measured at half of the length of the peak itself (Kübler, 1984; Chamley, 1989). Generally, high values of illite crystallinity indi-

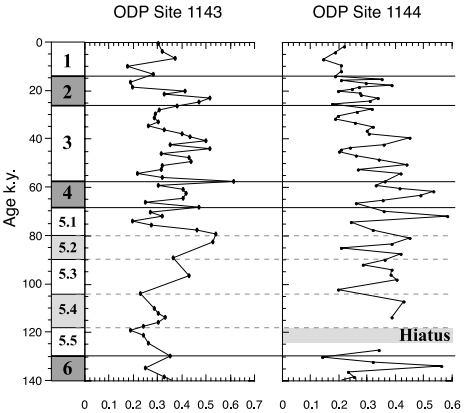

Fig. 5. Illite crystallinity from (a) Site 1143 and (b) Site 1144. Age and MIS as in Fig. 2. On average, values at Site 1144 are lower than at Site 1143 (0.32 and 0.34, respectively), indicating that illite is relatively less weathered at the northern site.

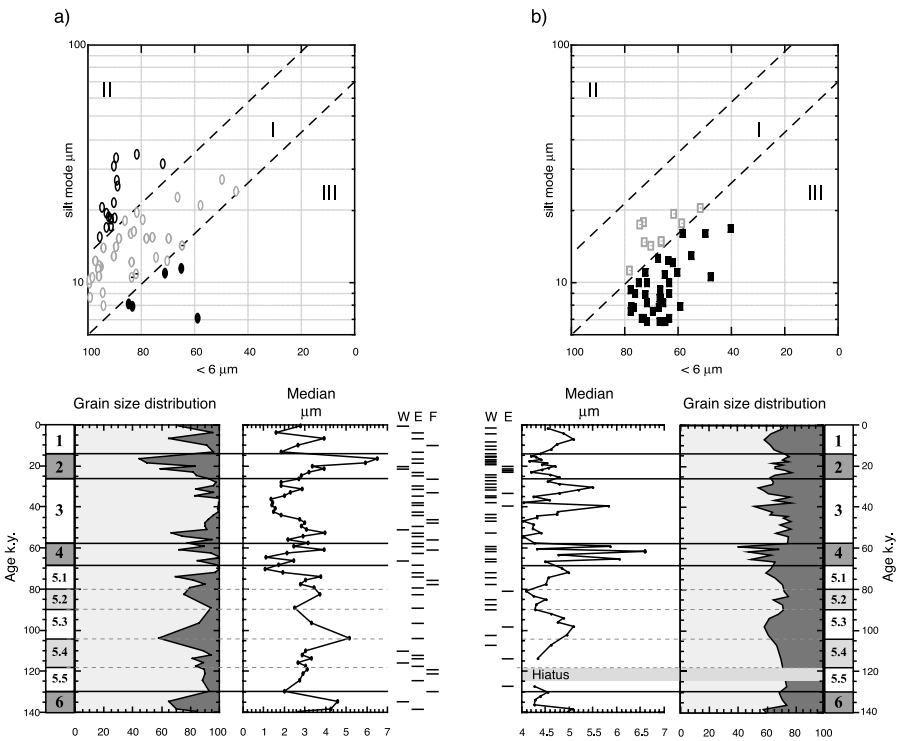

Fig. 6. Koopmann's diagram, grain-size distribution and median grain size for (a) Site 1143 and (b) Site 1144. In a Koopmann diagram, percentages of the fraction <6 μm and values of the silt mode (6–63 μm fraction) are plotted. The three fields indicate I = eolian (E), II = fluvial (F) and III = winnowed (W) sediments. The nature of the sediments as determined using Koopmann's diagram, is also reported on the side of the median grain-size graphs. In the grain-size distribution graphs, the <6 μm fraction is represented in light gray, while the 6–63 μm fraction is dark gray. Sediments at Site 1143 are clearly finer than at Site 1144.

cate highly degraded illites, while low values characterize relatively unaltered illites. Illite crystallinity from both sites exhibits comparable values (averaging 0.3) and similar trends, increasing toward stage 4 and then decreasing, reaching values of about 0.2, similar to stage 5.5 values, in the Holocene (Fig. 5).

3.3. Grain-size analysis

Fine material with particles <6 μm is more abundant at Site 1143 (more distal) than at Site 1144 (Fig. 6). This is also shown by the median (in volume) of the grains, averaging 3 μm for Site 1143, and 4.6 μm for Site 1144. Fine material contents are higher during interglacials and interstadials at Site 1143 (Fig. 6). Low values are observed during MIS 6, 4 and 2, when coarser material is up to more than 50%. The sediments are generally coarser at Site 1144. Visual inspection at the ESEM of selected samples showed that detrital material (quartz, phyllosilicates, and, to a lesser extent, plagioclases) is mainly concentrated in the <20 μm fraction. Fine material is abundant during stages 5 and 2 and at the base of stage 3. Silt and coarser sediments are present in high amounts during stage 4, at the top of stage 3 and during the Holocene (Fig. 6).

In order to characterize the nature of the sediments (eolian vs. fluvial vs. winnowed) at the two sites, we used the Koopmann index, which consists of an empirical relationship between the percentage of the siliciclastic fine fraction (<6 μm) and the modal grain size of the silt fraction (>6 μm; see Koopmann, 1981). This semi-quantitative approach was first used to study siliciclastic material deposited along the West African coast (Koopmann, 1981), and then employed to characterize sedment samples from the SCS (Wang et al., 1999). At Site 1143, eolian deposits are present throughout the sequence, but are more frequent during glacial stages. Fluvial sediments, characterized by less sorted material, are observed during interglacial stages 5.5, 5.1 and 1, but also during glacial periods (Fig. 6). At Site 1144, most of the samples fall in the field of winnowed sedi-

Table 2
Depth (mcd) and age (kyr) of peaks in median grain size from Sites 1143 and 1144 compared to age of peaks in quartz abundance (fraction >40 μm) from the Luochan Loess section

ODP 184-1143			ODP 184-1144			Luochan section	Notes
Depth (mcd)	Age (kyr)	Median grain size (μm)	Depth (mcd)	Age (kyr)	Median grain size (μm)	Age (kyr)	
0.32	6.76	3.95	3.8424	8.1	5.09		
0.77	16.35	6.5	14.043	16.82	4.4	15	1
0.92	18.32	5.95	16.974	18.44	4.52		
1.22	21.54	3.92	20.393	20.42	4.7	21.5	1
1.67	26.37	2.72	29	25.37	4.79	25.5–27.5	1
2.12	31.16	2.86	34.751	30.23	5.5	33.5–35	1
2.72	37.62	1.44	41.678	35.28	4.58		
			45.302	39.51	5.82	42–43.5	1
4.27	52.62	3.96	61.004	52.73	4.4	49.5–50.5	1
			67.449	59.19	5.86	58.5	1
4.87	60.67	3.94	70.204	61.73	6.59	61.5	1
			74.089	65.21	6.06	63.5–64	1
						66.5–67.5	1
6.07	75.69	3.78	80.598	72.01	4.98	69–71	2
6.52	82.34	3.74	89.899	85.02	4.51	81.3–84	2
			102.85	98.47	5.08	99.5–102	2
6.97	103.73	5.15					
7.42	113.84	3.3				113.5–115	2
7.87	119.24	3.13				119–121.6	2

1: Data from Porter and An (1995); 2: Data from An and Porter (1997).

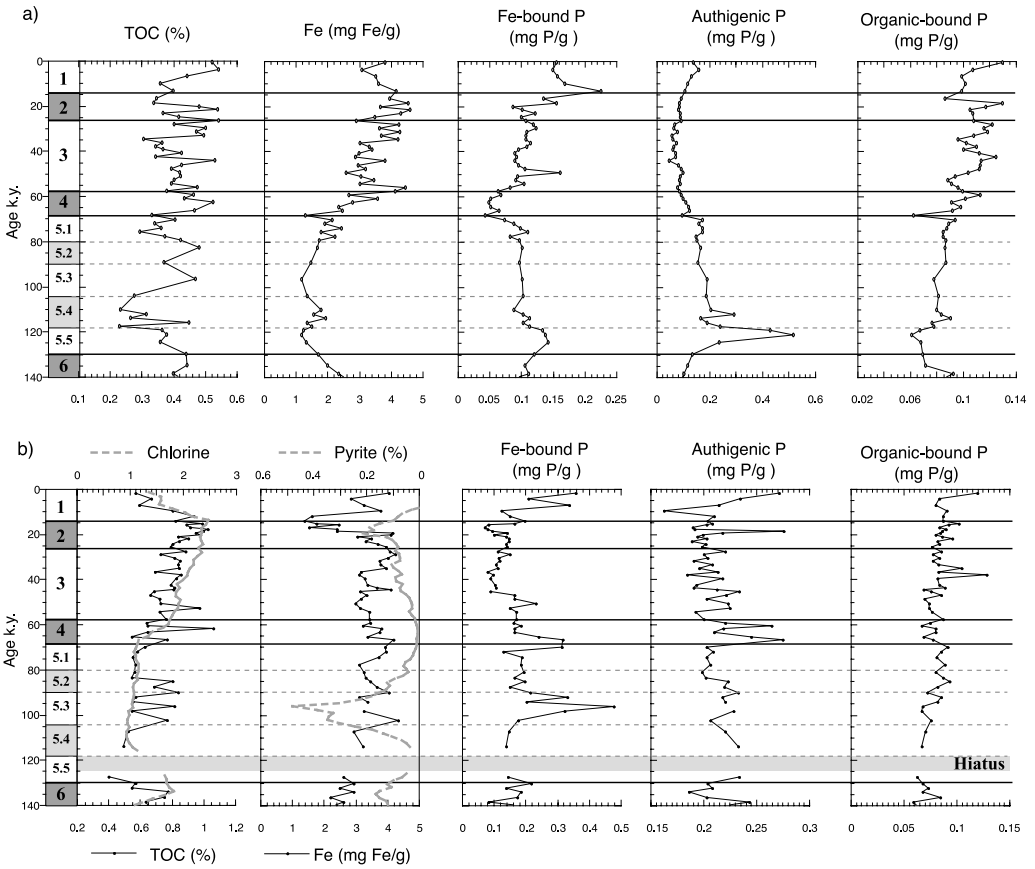

Fig. 7. Organic carbon percentage, Fe concentration, Fe-bound, authigenic and organic-bound phosphorus concentrations from (a) Site 1143 and (b) Site 1144. Age and MIS as in Fig. 2. For Site 1144, chlorins measured onboard are plotted against TOC %. Chlorin concentrations are given as relative abundance per gram dry weight (see Explanatory Notes in Wang et al., 2000). The smoothed record of pyrite percentages, determined by XRD, is plotted against ferric Fe. Raw data are not shown.

ments, eolian deposits are scarce and concentrated only during stage 2, while no sample falls in the field of fluvial deposits. At both sites, samples of the eolian field generally correspond to samples with higher median grain size. Despite the uncertainties due to stratigraphy, peaks in median grain size correspond between the two sites (Fig. 6 and Table 2).

3.4. Sediment geochemistry: sedimentary P and iron

Total phosphorus concentrations are about 1 mg P/g sediment at Site 1144 and not higher than 0.5 mgP/g at Site 1143. Authigenic P and the Fe-bound P are the most abundant phases at both sites (see Table 3), representing together

Table 3
Relative percentages of the different sedimentary phases of phosphorus

	Fe-bound P (%)	Authigenic P (%)	Detrital P (%)	Organic-bound P (%)
Site 184-1143	29	34	9	28
Site 184-1144	31	38	16	15

more than 60% of total P. The authigenic fraction is the most abundant at Site 1143, but the iron- and the organic-bound fractions are present in considerable amounts, and important variations in relative abundance are observed (Fig. 10). Detrital P represents on average only 9% of total P. Authigenic P, generally a carbonate–fluorapatite mineral (CFA), correlates to calcite, with high amounts occurring at the beginning of stage 5. Iron-bound P occurs in amounts around 0.1 mgP/g and at the beginning of stage 3 it increases to the maximum value of 0.22 mgP/g at around 14 ka. Organic-bound P decreases downward, probably associated with diagenesis and organic matter degradation.

Authigenic P in sediments from Site 1144 averages 0.22 mgP/g and represents 38% of total phosphorus. The steep increase at the top of the core can be linked to the precipitation of authigenic P or of a precursor mineral, which is consistent with high PO_4^{3-} pore water concentrations found at this site (see Site 1144 Inorganic Geochemistry chapter in Wang et al., 2000). Iron-bound P, the second most abundant P species at Site 1144, shows significant variations, with peaks during MIS 5.3, 4 and 1. Organic-bound P occurs in quantities comparable to Site 1143. Detrital P averages 0.7 mgP/g (Fig. 2). Ferric iron is present at relatively high amounts in both cores (on average 3 mg/g). At Site 1144, Fe concentrations show a pronounced minimum at the transition between stages 2 and 1.

Higher MARs of reactive P (sum of Fe-bound, authigenic and organic-bound P) are observed during glacial periods at both sites, but a maximum is recorded at the beginning of stage 5 at Site 1143, corresponding to peaks in calcite, and organic carbon MAR (Fig. 3). As for other index MARs, reactive P MARs at Site 1144 display a pronounced maximum at around 90 ka. Detrital P and Fe MAR are typically high during glacial periods at both sites. At Site 1144 Fe, detrital and reactive P MARs start decreasing before the end of stage 2, at around 20 ka (Fig. 3).

3.5. Organic carbon and $\delta^{15}N$

TOC at Site 1143 is low, between 0.2 and 0.5%.

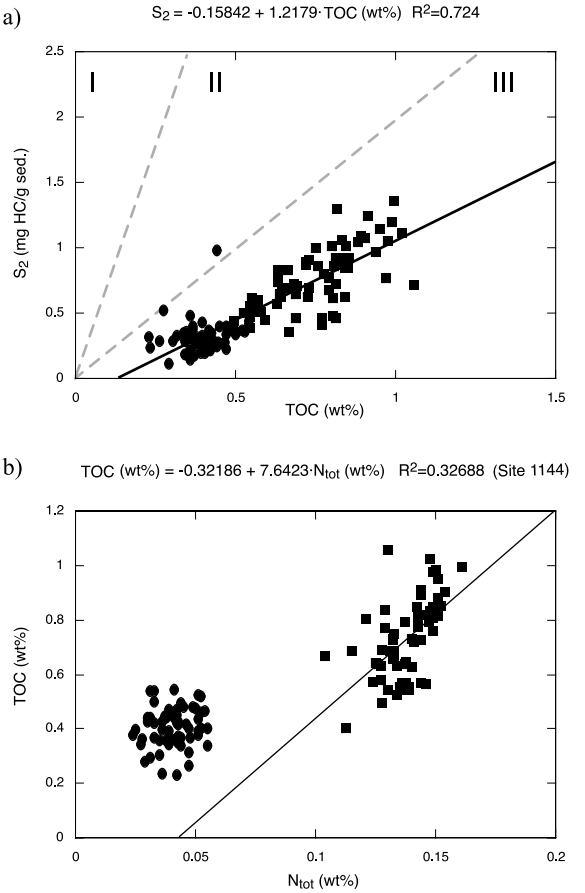

Fig. 8. (a) TOC % vs. S_2 values from Rock-Eval analysis. All samples fall in field III, indicating organic matter of continental origin. The correlation between the samples is significant. S_2 values from Rock-Eval should be taken with caution because of the low TOC content of the sample and the possible absorption of organic matter on clay minerals. (b) N_{tot} % vs. TOC % data from Site 1143 and Site 1144. Linear fitting for samples from Site 1143 (solid circles) yielded an extremely low correlation (not shown). The positive intercept of the *x*-axis for Site 1144 indicates that inorganic nitrogen is present, most likely adsorbed onto clay minerals. Samples from Site 1143 and Site 1144 are represented by solid circle and solid square symbols, respectively.

Prominent minima in the TOC curve are found during interstadial 5.4 and at the top of stage 2. The latter is associated with a minimum in organic-bound P. TOC at Site 1144 correlates with chlorin concentrations, considered as reflecting marine productivity (Higginson et al., 2003; Fig. 7). The correlation between chlorins, measured

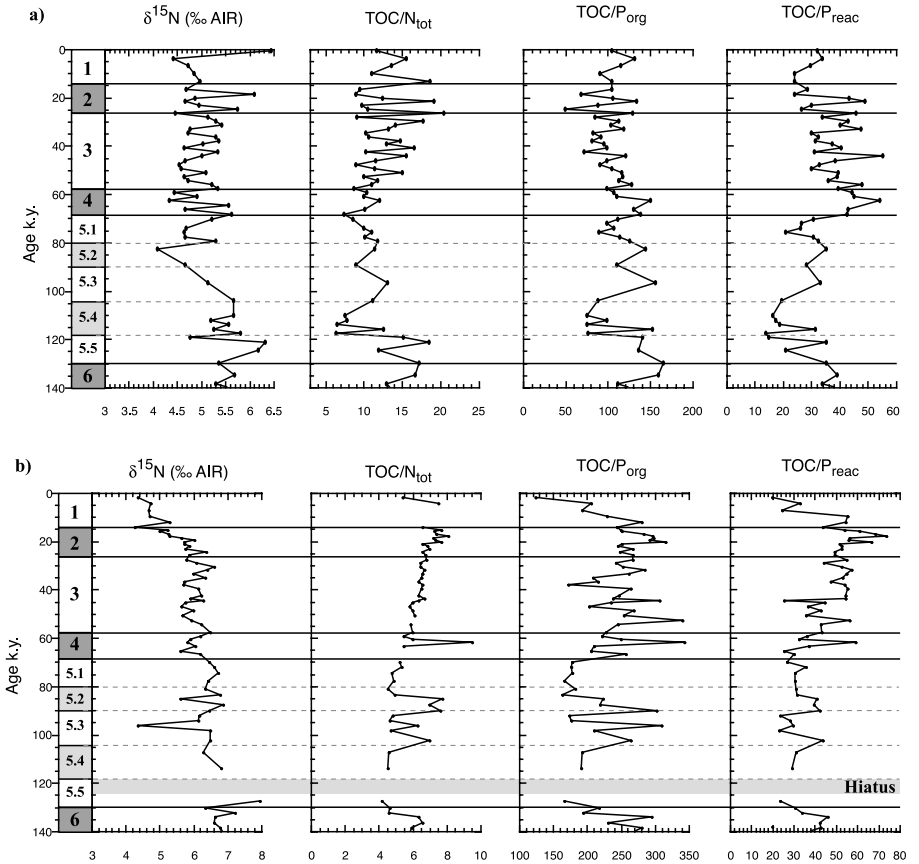

Fig. 9. Nitrogen isotope record, TOC/N_{tot}, TOC/P_{org} and TOC/P_{reac} molar ratios from (a) Site 1143 and (b) Site 1144. Age and MIS as in Fig. 2.

onboard (Wang et al., 2000), and TOC is not significant ($r^2 = 0.48$), but both records display a similar trend, which mimics detrital index variations. Organic matter MARs are similar to MARs of the other indices, showing highest values during glacial stages 4–2. A pronounced peak is observed at Site 1143 during stage 5.5, which correlates to the maximum in calcite MAR (Fig. 4).

The graph in Fig. 8a represents S_2 and TOC parameters from the Rock-Eval. As TOC % are quite low, above all for Site 1143, values should be interpreted with caution, but all samples fall in the type III kerogen field, which stands for terrestrial organic material (Langford and Blanc-Valleron, 1990). The negative y-axis intercept of the regression line calculated for all samples indicates adsorption by a mineral matrix, presumably clays (Langford and Blanc-Valleron, 1990). The samples, linearly distributed, display a significant correlation coefficient ($r^2 = 0.73$), pointing at a coherent group in terms of origin/source. Analysis of variance performed on HI values, which represent the S_2/TOC ratio and on average the slope of the regression curve of the S_2 vs. TOC graph, confirms that all samples belong to the same population. The TOC/organic phosphorus (TOC/P_{org}) ratio at Site 1143 is close to the TOC/P_{org} Redfield ratio (106, Redfield et al., 1963; or 117, Anderson and Sarmiento, 1994) for non-degraded phytoplankton material, while it is higher at Site 1144 (Fig. 9). TOC/total nitrogen (TOC/N_{tot}) molar ratio averages 11 for Site 1143 and 6 for Site 1144. Values at Site 1143 are quite high (up to 20) during stages 6, 5.5, 2 and the beginning of the

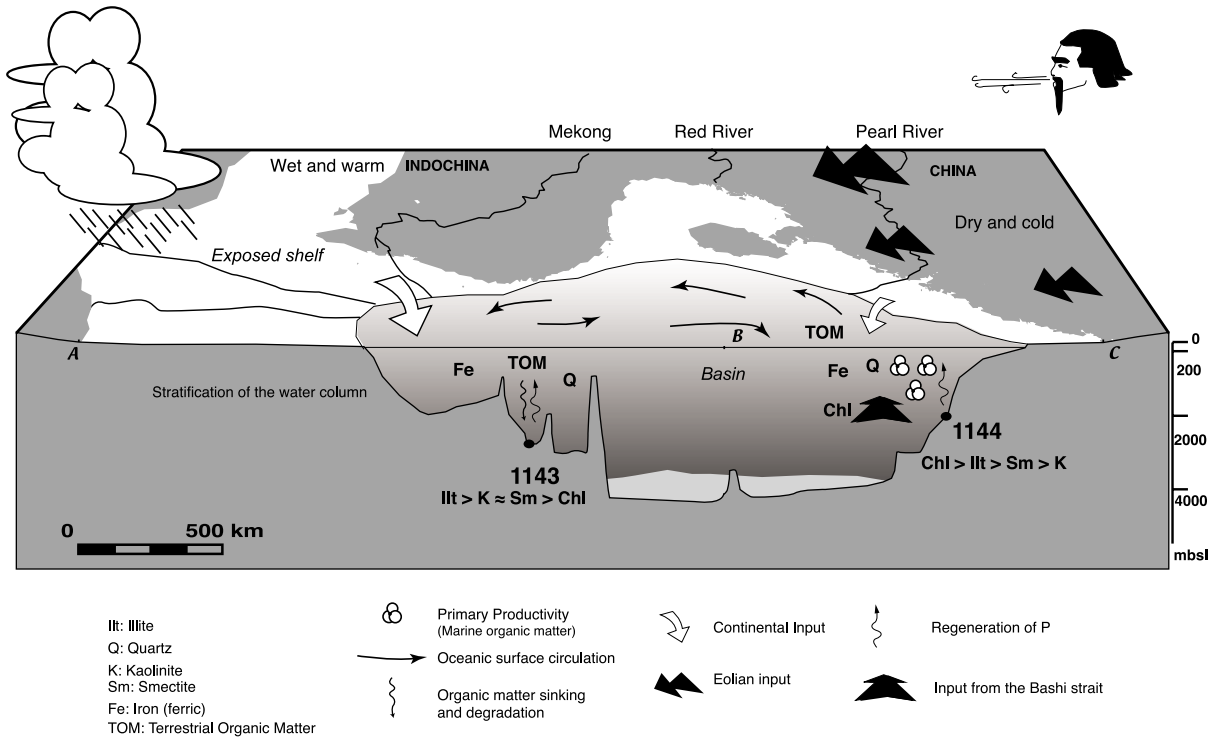

Fig. 10. Schematic model of the oceanographic, climatic and sedimentological situation of the SCS characterizing glacial periods, during the last 140 000 years. Glacial conditions are considered as denoted by strong winter monsoon activity and low sea level. Most of the continental shelf surrounding the SCS is exposed. See text and legend for details.

Holocene, while at Site 1144, highest values (up to 8) are observed during stages 5.3 and 5.2, stage 2 and the Holocene (Fig. 9).

$\delta^{15}N$ values from Site 1143 correlate with calcite, with higher values during interglacial periods (Figs. 2 and 9). At Site 1144, $\delta^{15}N$ presents more constant values, averaging 6‰. From around 20 ka to the top of the interval, the nitrogen isotope signature decreases to 4‰ (Fig. 9).

4. Discussion

4.1. Detrital material: key to weathering, oceanic and eolian circulation

Clay distribution in recent sediments from the SCS is controlled by provenance. Chen (1978) recognized seven different provinces, where the relative amount of clay minerals is determined by the mixing of clays coming from two main sources: the Asian continent, characterized by high contents of illite and chlorite, and the southern tropical islands, which, due to more humid and warm conditions, are characterized by important amounts of kaolinite and smectite. Relative variations of clay in time at these sites may be interpreted as resulting from changes in monsoonal regime, which affected weathering on the Asian continent, and in source, due to changes in oceanographic conditions.

Clay distribution at Sites 1143 and 1144 roughly corresponds to Chen's pattern: at Site 1144, clays from the northern Asian continent, e.g. illite and chlorite, are the main clay components. Illite and chlorite at Site 1143, which have probably the same origin as those at Site 1144, as suggested by the illite crystallinity and by triangular diagrams, are mixed with kaolinite and smectite, supplied from the surrounding tropical islands and by the weathering of volcanic rocks (Chen, 1978; Chamley, 1989).

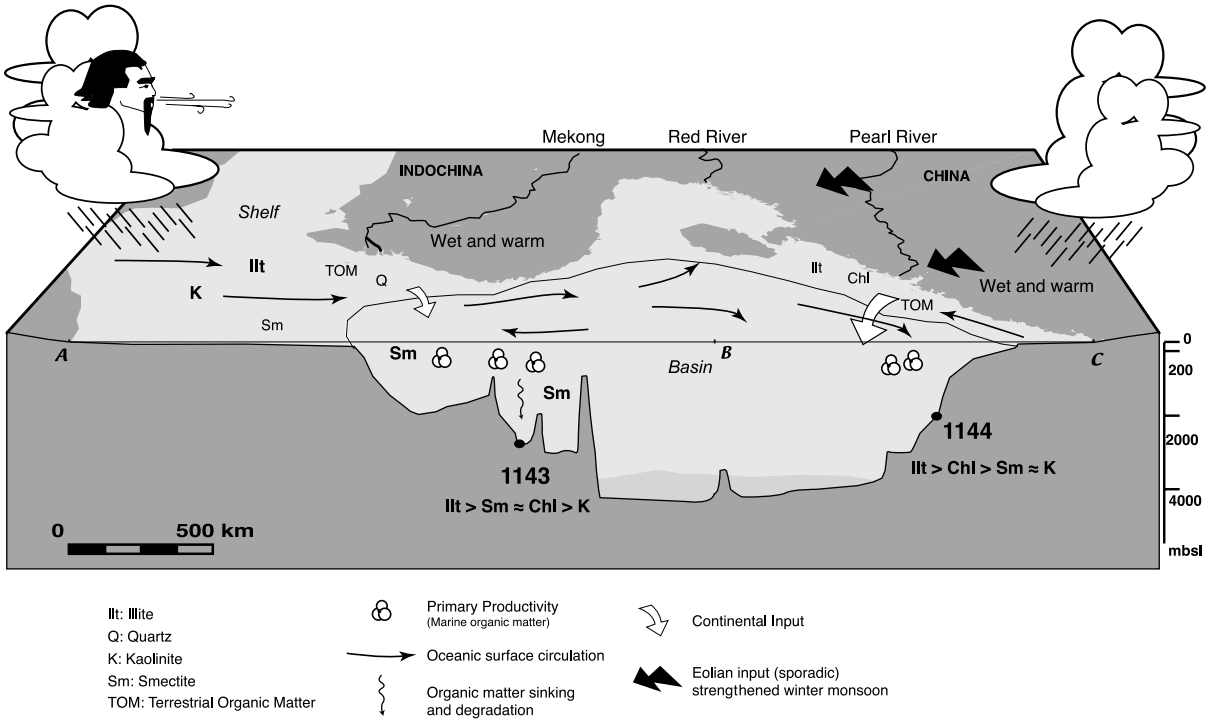

Fig. 11. Schematic model of the oceanographic, climatic and sedimentological situation of the SCS characterizing interglacial periods, during the last 140 000 years. Interglacial conditions are considered as denoted by strong summer monsoon activity and high sea level. See text and legend for details.

At Site 1143, clay distribution is fairly invariable during the last 140 kyr, and the most important changes are recorded during glacial periods, when kaolinite and, to a lesser extent, illite increased (Fig. 4). High values of kaolinite at Site 1143 are the result of (1) increased chemical weathering on the southern islands, due to the persistence of tropical climatic conditions (Wang et al., 1999); (2) increased eolian input from the interior of the Asian continent, characterized by dry climate; and (3) reworking of older sediments from the exposed Sunda shelf (Fig. 10). Quartz and iron are also higher during glacial periods, resulting from the enhanced eolian input from the Asian interior and from reworking of shelf sediments. MARs of detrital material clearly indicate increased accumulation during glacials (Fig. 3), confirming the hypothesis of strengthened erosion and enhanced eolian supply provided by clay minerals. Changes in grain size at Site 1143 are most likely related to the same factors: the establishment of the large Molengraaff River system and the increased winter monsoon strength could have provided coarser material to the site. Because both glacial and interglacial periods in the tropical regions of the SCS are characterized by humid and warm conditions, fluvial material contribution to Site 1143 is observed throughout the studied interval (Fig. 6).

Studies on modern sediments indicate that reworking of material from the Pearl River supply (Wang et al., 1999), and current transport from the ECS through the open Taiwan strait (Chen, 1978) should be considered as the main vectors responsible for clay and mineral distribution at Site 1144 (Fig. 11). During glacials, clay distribution at Site 1144 is opposite compared to Site 1143: low amounts of kaolinite and illite are paralleled by increased quantities of chlorites. During stages 2–4, conditions were more arid on the interior of the Asian continent, as also suggested by decresing illite crystallinity values. Thus, we

would expect illite contents to increase at Site 1144. But the closing of the Taiwan strait interrupted the input of material from the ECS shelf, whose sediments are rich in illite, and the connection between the SCS and the Pacific Ocean was only provided by the Bashi strait (Fig. 1). Surface sediments east of the coast of Luzon are rich in chlorite, because of the presence of chloritic schistose rocks, but relatively depleted in illite compared to Asian continent sediments (Kolla et al., 1980). Oceanic circulation during stages 4–2 could have prompted the transport of chlorite-enriched sediments from Luzon into the SCS, diluting the signal of the supply from the Asian continent (Fig. 10). As for Site 1143, MARs of detrital material at Site 1144 are highest during stages 2–4, and peaks correspond to peaks in median grain size, most likely related to enhanced eolian transport from the continent. Coarser material at around 9 ka could be the evidence of early Holocene strengthened summer monsoon, which could imply increased rainfall and consequent high fluvial input (Wang et al., 1999), which could have been transported to the site.

Despite the fact that Site 1144 is a site of focused sedimentation (Wang et al., 2000), where most of the deposits are originated by winnowing (Fig. 6b), and that Site 1143 is located far away from the continent (Fig. 1), episodes of strengthened eolian input are clearly recorded at both sites. Peaks in median at Site 1144 correlate within error with peaks at Site 1143 (Table 2). We observe a remarkable correspondence between the high values in the median grain size at both sites and peaks in quartz median diameter measured in the Luochan loess succession (Porter and An, 1995; An and Porter, 1997). Porter and An interpreted these features as representing periods of increased winter monsoon intensity and loess development also during interglacial periods, and they related them to cold events recorded in the North Atlantic region. As a matter of fact, eolian input to Site 1143 occurs also during interglacial stage 5, possibly during short-lasting cold periods, when winter monsoon was stronger. Also, high clay contents observed during stage 3 are probably related to eolian deposits, as indicated by Koopmann's classification (Fig. 6).

4.2. Organic matter and nutrients: key to productivity and sedimentation

Organic geochemical proxies (e.g. Rock-Eval indices, elemental ratios and stable isotope ratios of the organic matter) have been extensively used to determine both the nature and the degree of degradation of organic matter in marine sediments. Rock-Eval data and TOC/N_{tot} values indicate that organic material at Sites 1143 and 1144 is composed of a mixture of degraded terrestrial and marine organic matter (Figs. 8 and 9). Generally, TOC/N_{tot} ratios of sediments from Sites 1143 and 1144 average 6 and 11, respectively. The low correlation between TOC and total N at both sites ($r^2 = 0.019$ for Site 1143 and $r^2 = 0.327$ for Site 1144; Fig. 8b) implies that organic matter is constituted by a variable mixture of a terrestrial and a marine end-member. The difference in the TOC/N_{tot} ratios between the two sites is in agreement with the finding that sediments from Site 1144 bear an important percentage of inorganic nitrogen (see discussion below).

TOC/P_{org} ratios give contradictory information: while at Site 1144 TOC/P_{org} ratios are high (average of 250) and characteristic of a marine/terrestrial melange of organic material, TOC/P_{org} ratios at Site 1143 are close to the Redfield value. High organic P relative to organic carbon has been observed in various marine environments, especially in settings characterized by fine-grained sediments, as is the case for Site 1143 (Ruttenberg and Gõni, 1997). Sorption of organic P onto clay mineral surfaces may prevent remineralization of phosphorus and preferentially preserve it compared to organic carbon (Ruttenberg and Gõni, 1997). High values of TOC/P_{org} ratios at Site 1144 especially at around 100 ka and during cold stages 4–2 may reflect (1) the enhanced eolian input of terrestrial material during strengthened winter monsoon intervals, and (2) the preferential preservation of organic C compared to organic P, caused by low oxygen conditions in pore waters (Ingall and Jahnke, 1994).

Because degradation of organic material is considered as the main source of reactive P to pore waters and sediments (Broecker and Peng, 1982;

Froelich et al., 1982; Delaney, 1998), the TOC/P_{org} ratio is generally used to constrain the behavior of P in marine sediments and the nature of the organic matter (Anderson and Delaney, 2001). After degradation of the organic material, regenerated P is generally redistributed to different sedimentary phases or diffused back to the bottom water (Jarvis et al., 1994). Thus, the ratio between organic C and reactive P in sediments may give more detailed indications about environmental conditions and diagenetic processes in the sediments (e.g. Anderson and Delaney, 2001). TOC/P_{reac} ratios lower than the Redfield ratio indicate an excess of reactive P compared to organic carbon in sediments from both sites (Fig. 9). This surplus of P could be attributed to the presence of fish debris, as is the case for Oman margin sediments (Schenau et al., 2000), or to the supply of particulate phosphorus from the continent.

Relatively higher values of the TOC/P_{reac} ratios are observed during stages 2–4 at both sites, and, only at Site 1144, they parallel TOC/P_{org} ratio trend. This behavior may be explained either by reduced input of P to the SCS compared to interglacial intervals, or to regeneration and loss of P to the water column, due for instance to severe oxygen depletion and/or high alkalinity levels in pore waters, which may have hampered the precipitation of authigenic Ca–P (Ingall and Jahnke, 1994). High reactive P MARs during glacial periods, as well as other detrital index MARs, all indicate increased glacial continental contribution to sedimentation (Fig. 3), reasonably excluding the hypothesis of a decreased input of P during glacials. This suggests that dissolved regenerated P was probably recycled back to the water column. According to Wang et al. (1999) reduced circulation and increased oxygen deficiency in intermediate and bottom waters characterized glacial intervals in the SCS. Moreover, during those periods, Site 1144 was characterized by extremely high sedimentation rates (up to 2 m/kyr; see Bühring et al., in press), and the consistent eolian input of detrital material as well as organic matter, as testified by TOC MARs, could have reinforced already existent dysaerobic conditions, and raised alkalinity in pore waters. Glacials in the southern region of the SCS are characterized by a tropical climate, with enhanced precipitation and the establishment of the Molengraaff fluvial system. The enhanced input of fresh water, corroborated by the reconstruction of sea surface salinity (SSS) values using foraminifera (Wang et al., 1999, and references therein), may have triggered periodic stratification of the water column and consequent oxygen depletion.

Glacial–interglacial patterns of productivity at the two sites are different: upwelling occurs along the Vietnamese coast during summer monsoon periods (Wiesner et al., 1996), and evidence of the same phenomenon during interglacial times exists (i.e. $\delta^{13}C$ data of *G. ruber*, Wang et al., 1999). At Site 1143, high percentages of calcite are observed at the boundaries between stages 6–5 and 2–1, and persist all through stage 5.5 and the Holocene. Calcite MARs are high during stage 5.5, while relatively low values during glacial stages possibly imply diminished marine productivity due to weakened upwelling.

At Site 1144, high nutrient levels during glacials and deglaciation, resulting from strengthened eolian input of material from the continent (see MARs of Fe and detrital minerals) could have sustained high primary production. Despite the fact that TOC at this site is a mixture of marine and terrestrial organic matter, the similarity in trend between TOC concentration and chlorin concentrations may indicate high productivity during glacial and arid intervals, where the two records display the highest values and similarity (Fig. 7).

Provided adequate vertical mixing of the water column, regenerated nutrients such as phosphorus (see discussion above) could have helped in sustaining productivity. However, during glacial intervals, there is no evidence of upwelling at either site. Madhupratap et al. (1996) and Reichart et al. (1998) explained high productivity during winter monsoon season and glacial periods along the coasts of the Arabian Sea as the results of deep water mixing: the dry winter monsoon promoted evaporation, cooling of surface waters and consequent sinking, upwelling, thus nutrient-rich waters from down to 800 m. Since the winter monsoon strength increased during glacial times, it is not

excluded that the above process could have played a role also in the SCS, at least at Site 1144.

Recent studies on nitrate concentrations in SCS surface waters (for a review, see Kienast, 2000) indicate that nitrates are completely consumed by primary producers and that the SCS is consequently a nitrate-limited environment. Therefore, sedimentary $\delta^{15}N$ variability could be the expression of changes in circulation, of contribution of terrigenous organic material, denitrification, and/or nitrogen fixation (Altabet and Francois, 1994; Altabet et al., 1995; Farrell et al., 1995; Haug et al., 1998; Higginson et al., 2003). One major concern while studying nitrogen isotopes from clay-rich environments is the potential influence of inorganic nitrogen on the isotopic signature of the bulk sediment. To estimate this influence, data from both sites were plotted on a TOC wt% vs. N_{tot} wt% diagram (Fig. 8b; see Hedges et al., 1988). We performed statistical analysis on the distribution of the residuals (difference between each data point and its estimate) in order to use the correlation for data from Site 1144. The residuals show a normal distribution, so despite the low correlation coefficient ($r^2 = 0.327$ for Site 1144), we can confidently use the linear fit. The positive x-axis intercept for Site 1144 samples indicates that inorganic nitrogen, most likely sorbed on clay minerals, may account for at least 30% of the total nitrogen pool of these sediments. Sediments at this site are rich in clays whose main constituent of the fraction < 2 μm is illite (Fig. 4), which may incorporate ammonium (NH_4^+) at the place of K^+ in interlayer exchange sites (Schubert and Calvert, 2001). If the isotopic signal of sediments from Site 1144 were influenced by adsorption of inorganic nitrogen, low values of $\delta^{15}N$ should correspond to low values of the TOC/N_{tot} ratio, which is not the case (Fig. 9). $\delta^{15}N$ and TOC/N_{tot} ratios show opposite trends, as the low values in nitrogen isotopes observed during glacial stage 2 and the Holocene coincide with high values of the TOC/N_{tot} molar ratio (Fig. 9). This indicates that although inorganic nitrogen is present in sediments at Site 1144, $\delta^{15}N$ values bear information on the nature of the organic material.

At Site 1144, $\delta^{15}N$ values indicate that higher input of terrestrial organic material started probably before the boundary between stages 2 and 1, and continued throughout the Holocene, where nitrogen isotopes are lowest (Fig. 9). This could result from the flooding of the shelf and the consequent reworking and transport of terrestrial organic matter to deeper locations. At Site 1143, $\delta^{15}N$ values are almost invariable. During glacial stages 4–2, slightly low values (Fig. 9) may have recorded (1) an increased contribution of terrestrial organic matter, and (2) nitrogen fixation, due to complete utilization of nitrate if other nutrients are present (i.e. phosphorus and iron; Haug et al., 1998; Cullen, 1999; Tyrrell, 1999). The shift at stage 5.3 corresponds, in fact, to the increase of both TOC and detrital concentrations and MARs. In this scenario, the augmented input of material from land and the exposed shelf could also have led to elevated nutrient levels in surface water during glacials (Fig. 10).

The distribution of Fe-bound P is controlled mainly by redox conditions in the sediments, by variations in sedimentation rates, and the degree of crystallization of the Fe-oxides (Sundby et al., 1986; Van Cappellen and Ingall, 1994; Slomp, 1997). The lack of correlation ($r^2 = 0.0221$) observed at Site 1143 between ferric iron and Fe-bound P may be due to the presence of better crystallized detrital iron-oxides (Slomp et al., 1996; Schulz and Zabel, 2000): dissolved P is adsorbed in small concentrations on the surface of Fe-oxide-bearing minerals and it is released under reducing conditions, while a large part of well crystallized Fe-oxides is preserved. The upward increase of Fe-bound P may be the result of a larger amount of amorphous, diagenetically formed Fe-oxides compared to glacial periods, when Fe-oxides were provided by eolian and river input from the continent. The situation is far more complex at Site 1144, where the high sedimentation rates and the sediments rich in organic matter have promoted oxygen depletion in the sediments, reducing the adsorbing capacity of Fe-oxides. The most prominent peaks in Fe-bound P concentrations are strongly related to peaks in sedimentation rates, as is the case for the interval at around 100 ka and during stage 4 (Fig. 7). High sedimentation rates may hasten the

burial of sediments and P adsorbed on Fe-oxides may have been preserved.

The ferric Fe record at Site 1144 presents a well-defined minimum at the stage 2–1 boundary, already below the zone of sulfate reduction (see Inorganic Geochemistry chapter, Site 1144 in Wang et al., 2000), which corresponds to a maximum in authigenic pyrite (Fig. 7), and to a minimum in magnetic susceptibility (see Kissel et al., 2003). At the base of this minimum, where pyrite percentages are higher, Fe-bound P is low, possibly recording important changes in sedimentation. Post-depositional enrichments of Fe sulfides, such as authigenic pyrite, have already been observed in other sedimentary environments (i.e. the Amazon deep-sea fan, Kasten et al., 1998). The process responsible for this phenomenon is believed to be the installation of a non-steady-state diagenetic regime, promoting the precipitation of authigenic minerals. Kasten and co-authors recognized the significant drop in sedimentation rates and in organic carbon accumulation characterizing the transition between stage 2 and the Holocene as the controlling factor (Kasten et al., 1998). As is also observed for Site 1144, the boundary between stages 2 and 1 is marked by a four-fold decrease in sedimentation rates (Bühring et al., in prep.). The decreased sedimentation rate, as inferred both by isotopic stratigraphy and sedimentary geochemistry at Site 1144, may indicate that sea level started rising already during the last interval of stage 2. Tropical sea-level records south of 35°N clearly indicate that sea-level changes after the Last Glacial Maximum may have begun as early as 18 ka (Winkler and Wang, 1993).

4.3. Toward a reliable proxy for monsoon activity?

One important issue in studying monsoon systems in the past is to determine a reliable proxy which excusively records monsoon variability through time, without being affected by other processes. In this study, we have presented several mineralogical, organic and inorganic geochemical proxies from two different locations in the SCS, which have recorded changes during the last 140 000 years. It is clear to us that most of them are not direct indicators of the monsoon history.

Because of the geographic and bathimetric configuration of the SCS, this basin is extremely sensitive to eustatic changes, which were recorded by many proxies. Eolian input from the continent is generally mixed with material reworked from the shelf, and sometimes it is not straightforward to unravel the 'true' monsoon signal. Only a careful comparison between all the proxies at the two sites helped in understanding the evolution of climate and monsoon during the last glacial–interglacial cycle in the SCS. From our study, the best proxy to infer eolian input and reconstruct winter monsoon activity and strength seems to be provided by the median grain size and the use of Koopmann's classification (Fig. 6). As discussed previously, peaks in median grain size correlate between the two sites and are in agreement with the age of intervals of enhanced winter monsoon recorded in Chinese loess sections (Porter and An, 1995; An and Porter, 1997).

5. Conclusions

The multiproxy study of sediments from ODP Sites 1143 and 1144 provides new information on the evolution of sedimentation and climate in the SCS area during the last glacial–interglacial cycle. The complex interplay of monsoonal climate, which controls river and eolian input as well as current circulation, and sea-level variations, linked to global climate changes, drives the distribution of sediments, nutrients, and organic matter in the SCS.

(1) Interglacial periods are characterized by high sea level, which permitted the connection of the SCS both with the Indian and the Pacific oceans. The circulation in the SCS was controlled by wind direction and by the overturn between summer and winter monsoons. Sediments were derived from the Asian continent, the tropical islands surrounding the SCS, and the ECS, brought in by the inflow through the Taiwan strait. High productivity was fostered by the presence of upwelling cells close to Site 1143 and by fluvial input of nutrients. Short arid and cold periods, characterized by enhanced eolian input, were common

and possibly correlated with a more global climatic variability.

(2) During glacial stages, sea level was about 120 m lower than during interglacial periods, changing the configuration of the basin. Most of the connections with the open ocean were shut down, oceanographic circulation changed, and the wide Sunda shelf was exposed and drained by the large Molengraaff fluvial system. Sediments previously deposited on the shelf were reworked and deposited in deeper areas, and the changed current system brought into the sites sediments from other sources than the interglacial ones. Arid conditions on the interior of the Asian continent promoted the development of loess deposition, and the strengthened winter monsoon brought high amounts of detrital material and nutrients to the SCS. Generally reduced circulation, stratification of the water column, in the southern SCS, and high organic carbon flux, in the northern SCS, fostered severe oxygen depletion in bottom waters and high alkalinity in pore waters. These conditions hampered precipitation of authigenic phosphorus, which was released from the sediments and, provided there was sufficient vertical mixing, re-diffused to the water column.

(3) The transition between stages 2 and 1 was marked by a severe drop in sedimentation rates, and, within the error given by isotopic stratigraphy uncertainty, the sea level started to rise as early as 18 ka. The Holocene was characterized by the re-establishment of humid conditions all over the Asian continent and of open circulation and connection with the Indian and Pacific oceans.

Similar multiproxy studies of sediments from the SCS at higher time resolution are now needed to assess the importance and the extent of these processes and of the related feedback mechanisms, and the connection (leads and lags) with other climate forcing factors (atmosphere and ocean circulation, Milankovitch cycles).

Acknowledgements

The authors would like to express their gratitude to the captain, the crew and the technical staff of ODP Leg 184, for their precious help and assistance. F.T. thanks J. Tian, P. Wang, C. Bürhing and M. Sarnthein for kindly providing the isotopic stratigraphy for Sites 1143 and 1144. The authors gratefully thank J. Richard, K. Hamila and H. Paul for preparation of samples and help in laboratory work. This research used samples and data provided by the Ocean Drilling Program (ODP). ODP is sponsored by the U.S. National Science Foundation (NSF) and participating countries under management of Joint Oceanographic Institutions (JOI), Inc. This study was supported by the University of Neuchâtel, Switzerland.

References

Altabet, M.A., Francois, R., 1994. Sedimentary nitrogen isotopic ratio as a recorder for surface ocean nitrogen utilization. Glob. Biogeochem. Cycles 8, 103–116.

Altabet, M.A., Francois, R., Murray, D.W., Prell, W.L., 1995. Climate-related variations in denitrification in the Arabian Sea from sediment 15N/14N ratios. Nature 373, 506–509.

An, Z.S., 2000. The history and variability of the East Asian paleomonsoon climate. Quat. Sci. Rev. 19, 171–187.

An, Z.S., Porter, S.C., 1997. Millennial-scale climatic oscillations during the last interglaciation in central China. Geology 25, 603–607.

Anderson, L.A., Sarmiento, J.L., 1994. Redfield ratios of remineralization determined by nutrient data analysis. Glob. Biogeochem. Cycles 8, 65–80.

Anderson, L.D., Delaney, M.L., 2000. Sequential extraction and analysis of phosphorus in marine sediments: Streamlining of the SEDEX procedure. Limnol. Oceanogr. 45, 509–515.

Anderson, L.D., Delaney, M.L., 2001. Carbon to phosphorus ratios in sediments: implications for nutrient cycling. Global Biogeochemical Cycles 15, 65–79.

Broecker, W.S., Peng, T.-H., 1982. Tracers in the Sea. Lamont-Doherty Geological Observatory, Palisades, NY.

Bühring, C., Sarnthein, M., Erlenkeuser, H., in press. Toward a high-resolution stable isotope stratigraphy of the last 1.1 million years: Site 1144, South China Sea. Proc. ODP Sci. Results.

Chamley, H., 1989. Clay Sedimentology. Springer, New York.

Chen, P.-Y., 1978. Minerals in bottom sediments of the South China Sea. Geol. Soc. Am. Bull. 89, 211–222.

Cullen, J., 1999. Iron, nitrogen and phosphorus in the ocean. Nature 402, 372.

Delaney, M.L., 1998. Phosphorus accumulation in marine sediments and the oceanic phosphorus cycle. Glob. Biogeochem. Cycles 12, 563–572.

Eaton, A.D., Clesceri, L.S., Greenberg, A.E. (Eds.), Standard Methods for the Examination of Water and Wastewater, 19th edn. APHA, Washington, DC.

Espitalié, J., Deroo, G., Marquis, F., 1986. La pyrolyse Rock-Eval et ses applications - III partie. Rev. Inst. Fr. Pet. 41, 73–89.

Farrell, J.W., Pedersen, T.F., Calvert, S.E., Nielsen, B., 1995. Glacial-interglacial changes in nutrient utilization in the equatorial Pacific Ocean. Nature 377, 514–517.

Froelich, P.N., Bender, M.L., Luedtke, N.A., Heath, G.R., De Vries, T., 1982. The marine phosphorus cycle. Am. J. Sci. 282, 474–511.

Haug, G.H., Pedersen, T.F., Sigman, D.M., Calvert, S.E., Nielsen, B., Peterson, L.C., 1998. Glacial/interglacial variations in production and nitrogen fixation in the Cariaco Basin during the last 580 kyr. Paleoceanography 13, 427–432.

Hedges, J.I., Clark, W.A., Cowie, G.L., 1988. Organic matter sources to the water column and surficial sediments of a marine bay. Limnol. Oceanogr. 33, 1116–1136.

Higginson M.J., Altabet, M.A., Maxwell, J.R., 2003. Nitrogen isotope and chlorin paleoproductivity records from the northern South China Sea: remote versus local forcing of millennial- and orbital-scale variability. Mar. Geol. 201, doi:10.1016/S0025-3227(03)00218-4, this issue.

Huang, C.-Y., Liew, P.-M., Zhao, M., Chang, T.-C., Kuo, C.-M., Chen, M.-T., Wang, C.-H., Zheng, L.-F., 1997. Deep sea and lake records of the Southeast Asian paleomonsoons for the last 25 thousand years. Earth Planet. Sci. Lett. 146, 59–72.

Ingall, E., Jahnke, R., 1994. Evidence for enhanced phosphorus regeneration from marine sediments overlain by oxygen depleted waters. Geochim. Cosmochim. Acta 58, 2571–2575.

Jarvis, I., Burnett, W.C., Nathan, Y., Almbaydin, F.S.M., Attia, A.K.M., Castro, L.N., Flicoteaux, R., Hilmy, M.E., Husain, V., Qutawnah, A.A., Serjani, A., Zanin, Y.N., 1994. Phosphorite geochemistry: state-of-art and environmental concerns. Eclogae Geol. Helv. 87, 643–700.

Kasten, S., Freudenthal, T., Gingele, F.X., Schulz, H.D., 1998. Simultaneous formation of iron-rich layers at different redox boundaries in sediments of the Amazon deep-sea fan. Geochim. Cosmochim. Acta 62, 2253–2264.

Kienast, M., 2000. Unchanged nitrogen isotopic composition of organic matter in the South China Sea during the last climatic cycle: Global implications. Paleoceanography 15, 244–253.

Kissel, C., Laj, C., Clemens, S., Solheid, P., 2003. Magnetic signature of environmental changes in the last 1.2 my at ODP Site 1146, South China Sea. Mar. Geol. 201, doi:10.1016/S0025-3227(03)00212-3, this issue.

Kolla, V., Nadler, L., Bonatti, E., 1980. Clay mineral distributions in surface sediments of the Philippine Sea. Oceanol. Acta 3, 245–250.

Koopmann, B., 1981. Saharan dust deposition in the subtropical Atlantic during the last 25,000 years (in German). Meteor Forschungsergeb. C 5, 23–54.

Kübler, B., 1984. Les indicateurs des transformations physiques et chimiques dans la diagenèse. Temperature et calorimetrie., Thermométrie et barométrie géologique. Soc. Fr. Minér. Cristallogr., Paris, pp. 489–596.

Kübler, B., 1987. Dosage quantitatif des minéraux majeurs des roches sédimentaires par diffraction X. Cah. Inst. Géol. Neuchâtel, Série ADX.

Lafargue, E., Espitalié, J., Marquis, F., Pillot, D., 1996. Rock Eval 6: applications in hydrocarbon exploration, production and in soil contamination studies. Latin American Congress on Organic Geochemistry, Cancun.

Langford, F.F., Blanc-Valleron, M.-M., 1990. Interpreting Rock-Eval pyrolysis data using graphs of pyrolizable hydrocarbons vs. total organic carbon. AAPG 74, 799–804.

Madhupratap, M., Prasanna Kumar, S., Bhattathiri, P.M.A., Dileep Kumar, M., Raghukumar, S., Nair, K.K.C., Ramaiah, N., 1996. Mechanism of the biological response to winter cooling in the northeastern Arabian Sea. Nature 384, 549–552.

Moore, D.M., Reynolds, R.C.J., 1997. X-Ray Diffraction and the Identification and Analysis of Clay Minerals. Oxford University Press.

Oinuma, K., Shimoda, S., Sudo, T., 1972. Triangular diagrams of surveying chemical composition of chlorites. J. Tokyo Univ. 15, 1–13.

Pelejero, C., Kienast, M., Wang, L., Grimalt, J.O., 1999. The flooding of Sundaland during the last deglaciation: imprints in hemipelagic sediments from the southern South China Sea. Earth Planet. Sci. Lett. 171, 661–671.

Porter, S.C., An, Z., 1995. Correlation between climate events in the North Atlantic and China during the last glaciation. Nature 375, 305–308.

Prell, W.L., Kutzbach, J.E., 1992. Sensitivity of the Indian monsoon to forcing parameters and implications for its evolution. Nature 360, 647–652.

Redfield, C.C., Ketchum, B.H., Richards, F.A., 1963. The influence of organisms on the composition of sea-water. In: Hill, M.N. (Ed.), The Sea. Wiley-Interscience, New York, pp. 26–77.

Reichart, G.J., Lourens, L.J., Zachariasse, W.J., 1998. Temporal variability in the northern Arabian Sea Oxygen Minimum Zone (OMZ) during the last 225,000 years. Paleoceanography 13, 607–621.

Rey, M., Kübler, B., 1983. Identification des micas des séries sédimentaires par diffraction X, à partir de la série harmonique (001) des préparation orientées. Bull. Suisse Minér. Pétrogra. 63, 13–36.

Ruttenberg, K.C., 1992. Development of a sequential extraction method for different forms of phosphorus in marine sediments. Limnol. Oceanogr. 37, 1460–1482.

Ruttenberg, K.C., Gõni, M.A., 1997. Phosphorus distribution, C:N:P ratios, and $\delta^{13}C_{oc}$ in artic, temperate, and tropical coastal sediments: tools for characterizing bulk sedimentary organic matter. Mar. Geol. 139, 123–145.

Schenau, S.J., Slomp, C.P., De Lange, G.J., 2000. Phosphogenesis and active phosphorite formation in sediments from the Arabian Sea oxygen minimum zone. Mar. Geol. 169, 1–20.

Schönfeld, J., Kudrass, H.-R., 1993. Hemipelagic sediment accumulation rates in the South China Sea related to late quaternary sea-level changes. Quat. Res. 40, 368–379.

Schubert, C.J., Calvert, S.E., 2001. Nitrogen and carbon isotopic composition of marine and terrestrial organic matter in Arctic Ocean sediments: implications for nutrient utilization and organic matter composition. Deep-Sea Res. I 48, 789–810.

Schulz, H.D., Zabel, M., 2000. Marine Geochemistry. Springer, Berlin, 455 pp.

Sirocko, F., Garbe-Schönberg, D., McIntyre, A., Molfino, B., 1996. Teleconnections between the subtropical monsoons and high-latitudes climates during the last deglaciation. Science 272, 526–529.

Slomp, C.P., 1997. Early diagenesis of phosphorus in continental margin sediments. Ph.D. Thesis, Den Burg, Texel, 178 pp.

Slomp, C.P., Epping, E.H.G., Helder, W., van Raaphorst, W., 1996. A key role of iron-bound phosphorus in authigenic apatite formation in North Atlantic continental platform sediments. J. Mar. Res. 54, 1179–1205.

Sundby, B., Anderson, L.G., Hall, P.O.J., Iverfeldt, A., Van der Loeff, M.M.R., Westerlund, S.F.G., 1986. The effect of oxygen on release and uptake of cobalt, manganese, iron and phosphate at the sediment-water interface. Geochim. Cosmochim. Acta 50, 1281–1288.

Tian, J., Wang, P., Cheng, X., Li, Q., 2002. Astronomically tuned Plio-Pleistocene benthic $\delta^{18}O$ record from South China Sea and Atlantic-Pacific comparison. Earth Planet. Sci. Lett. 203, 1015–1029.

Tyrrell, T., 1999. The relative influences of nitrogen and phosphorus on oceanic primary production. Nature 400, 525–531.

Van Cappellen, P., Ingall, E.D., 1994. Benthic phosphorus regeneration, net primary production, and ocean anoxia: a model of the coupled marine biogeochemical cycles and phosphorus. Paleoceanography 9, 677–698.

Wang, L., Oba, T., 1998. Tele-connections between East Asian Monsoon and the High-latitude climate: A comparison between the GISP 2 ice core record and the high resolution marine records from the Japan and the South China Sea. Quat. Res. 37, 211–219.

Wang, L., Sarnthein, M., Erlenkeuser, H., Grimalt, J., Grootes, P., Heilig, S., Ivanova, E., Kienast, M., Pflaumann, U., 1999. East Asian Monsoon climate during the Late Pleistocene: high-resolution sediment records from the South China Sea. Mar. Geol. 156, 245–284.

Wang, L., Wang, P., 1990. Late Quaternary paleoceanography of the South China Sea: glacial-interglacial contrasts in an enclosed basin. Paleoceanography 5, 77–90.

Wang, P., Prell, W.L., Blum, P., Arnold, E.M., Buehring, C.J., Chen, M.-P., Clemens, S.C., Clift, P.D., Colin, C.J.G., Farrell, J.W., Higginson, M.J., Zhimin, J., Kuhnt, W., Laj, C.E., Lauer-Leredde, C., Leventhal, J.S., Anchun, L., Qingmou, L., Jian, L., McIntyre, K., Miranda, C.R., Nathan, S.A., Shyu, J.-P., Solheid, P.A., Xin, S., Tamburini, F., Trentesaux, A., Wang, L., Nessler, S., Green, L.E., 2000. Proc. ODP Init. Repts. 184.

Wang, P., Wang, L., Yunhua, B., Zhimi, J., 1995. Late Quaternary paleoceanography of the South China Sea: surface circulation and carbonate cycles. Mar. Geol. 127, 145–165.

Webster, P.J., 1987. The elementary monsoon. In: Fien, J., Stephens, P. (Eds.), Monsoon. Wiley, New York, pp. 3–32.

Wiesner, M.G., Zheng, L., Wong, H.K., Wang, Y., Chen, W., 1996. Fluxes of particulate matter in the South China Sea. In: Ittekkot, V., Schäfer, P., Honjo, S., Depetris, P.J. (Eds.), Particle Flux in the Ocean. Wiley, pp. 293–312.

Winkler, M.G., Wang, P.W., 1993. The Late-Quaternary vegetation and climate of China. In: Wright, H.E.J., et al. (Eds.), Global Climate since the Last Glacial Maximum. University of Minnesota Press, pp. 221–261.